



Swansea University
Prifysgol Abertawe



Cronfa - Swansea University Open Access Repository

This is an author produced version of a paper published in :
International Journal of Fatigue

Cronfa URL for this paper:

<http://cronfa.swan.ac.uk/Record/cronfa5832>

Paper:

Lancaster, R., Steele, A., Evans, J., Jones, N. & Whittaker, M. (2009). Plain and notched fatigue in nickel single crystal alloys. *International Journal of Fatigue*

<http://dx.doi.org/10.1016/j.ijfatigue.2009.03.010>

This article is brought to you by Swansea University. Any person downloading material is agreeing to abide by the terms of the repository licence. Authors are personally responsible for adhering to publisher restrictions or conditions. When uploading content they are required to comply with their publisher agreement and the SHERPA RoMEO database to judge whether or not it is copyright safe to add this version of the paper to this repository.

<http://www.swansea.ac.uk/iss/researchsupport/cronfa-support/>

Plain and Notched Fatigue in Nickel Single Crystal Alloys

W.J. Evans¹, R. Lancaster¹, A. Steele¹, M. Whittaker¹ and N. Jones²

¹Materials Research Centre, School of Engineering, Swansea University, Singleton Park,
Swansea SA2 8PP

²Rolls-Royce plc, P O Box 31, Elton Road, Derby, DE24 8BJ

Keywords: CMSX-4, Alloy variants, strain control fatigue, notch fatigue, casting pores, life prediction

Abstract

The paper focuses on CMSX-4 and two experimental alloys, LDSX-5 and LDSX-6, developed to provide alternative performance attributes. The specific objective in this work was an exploration of the Low Cycle Fatigue (LCF) characteristics of these three alloy variants and the assessment of methods for predicting the observed lives. A comparison of the alloys is presented in relation to their strain control fatigue response and notch fatigue behaviour. Predictions of notch lives are made from the plain specimen data but found to be extremely pessimistic at the lower temperature studied, 650°C. The inaccuracies are attributed to the presence of casting pores. Using measured crack growth data and pore sizes, it is shown that fracture mechanics calculations of residual lives are more appropriate. At 800°C, the higher temperature studied, Walker strain predictions of notch lives are more meaningful. This is explained in terms of the relaxation of stresses at the defects.

Introduction

The research programme set out to explore the LCF behaviour of experimental single crystal nickel alloys. The alloys specifically focused on alternative compositions to CMSX-4 that offer various performance attributes. The two alloys highlighted in the present paper were chosen because of lower densities, improved stability (LDSX-5) and enhanced creep strength (LDSX-6). Data generated on CMSX-4 were used for comparison. All alloys were produced with a [100] orientation using conventional single crystal casting technology. The experiments involved plain and notched test-pieces with K_t values of 2.38 for a centre hole plus 2.3 and 3.6 for double edge notch geometries. Plain specimens were subjected to 15cpm strain control fatigue with R values of 0 and -1. From these tests, hysteresis loops were recorded and cyclic stress-strain curves constructed. The notch specimens were tested with the same waveform at R=0. Plain and notched specimens were evaluated at 650°C and 800°C. The orientations of test-pieces and notches were confirmed to be consistent by means of Electron Back-Scatter Diffraction (EBSD) measurements.

A prime objective of the work was the assessment of methods for predicting fatigue performance. In particular, the Walker strain relationship has previously been shown to provide an effective means of predicting notch behaviour [1, 2]. In the present situation, however, inconsistencies were identified which were attributed to the presence of casting pores. These defects introduced the need to consider an alternative damage tolerance

approach based on fracture mechanics and the application of crack growth rate data. Both life prediction methods are highlighted and discussed.

Experimental Procedures

The Alloys

The compositions of the LDSX-5 and LDSX-6 alloys are summarised in Table 1 in relation to CMSX-4.

Table I. Alloy Compositions (wt%)

| | Co | Cr | Mo | W | Re | Ru | Al | Ti | Ta | Hf |
|--------|-----|-----|-----|-----|-----|-----|-----|-----|-----|-----|
| LDSX-5 | 8.4 | 3.1 | 2.7 | 2.9 | 6.4 | 4.6 | 5.6 | 0.3 | 6.5 | 0.1 |
| LDSX-6 | 3.1 | 3.3 | 2.7 | 4.8 | 6.4 | 4.7 | 5.6 | 0.3 | 6.5 | 0.1 |
| CMSX-4 | 9 | 6.4 | 0.6 | 6.4 | 3 | 0 | 5.6 | 1 | 6.5 | 0.1 |

The principal differences from CMSX-4 are a higher rhenium content, the addition of ruthenium, greater amount of molybdenum and reduced tungsten particularly for LDSX5. This is illustrated in figure 1. These changes influenced density, stability, creep strength and castability. The relative benefits are highlighted in Table 2.

Table II. Relative attributes of the alloys

| | | | | | |
|----------------|--------|---|--------|---|--------|
| Stability | LDSX-5 | > | LDSX-6 | > | CMSX-4 |
| Creep strength | CMSX-4 | > | LDSX-6 | > | LDSX-5 |
| Castability | CMSX-4 | > | LDSX-5 | > | LDSX-6 |

Following casting the alloys were solution treated at 1340°C, gas-fan quenched, primary aged at 1150°C, quenched and finally aged at 870°C. Microstructures were defined by etching in 10ml HNO₃, 50ml HCl, 2.5g CuCl₂ and 40ml H₂O. Scanning Electron Microscopy (SEM) comparisons of CMSX-4, LDSX-5 and LDSX-6 at the same magnification are reproduced in figures 2a, 2b and 2c.

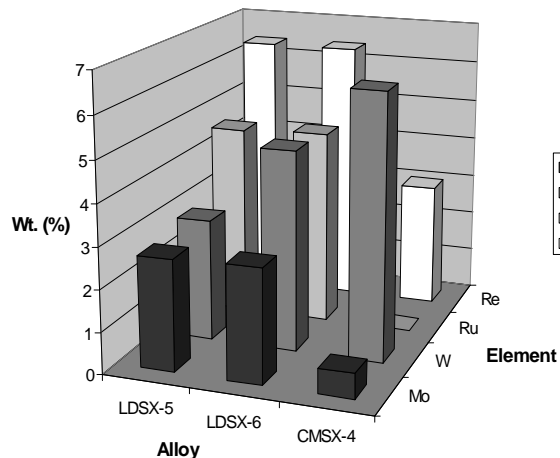


Figure 1. Single crystal material compositions

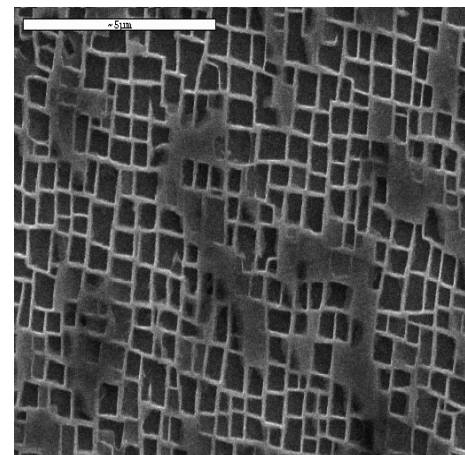


Figure 2a. Microstructure of CMSX-4

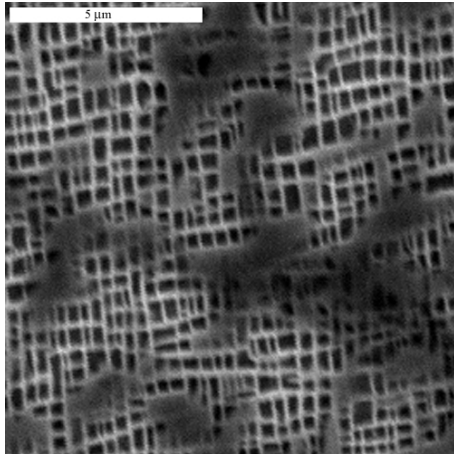


Figure 2b. Microstructure of LDSX-5

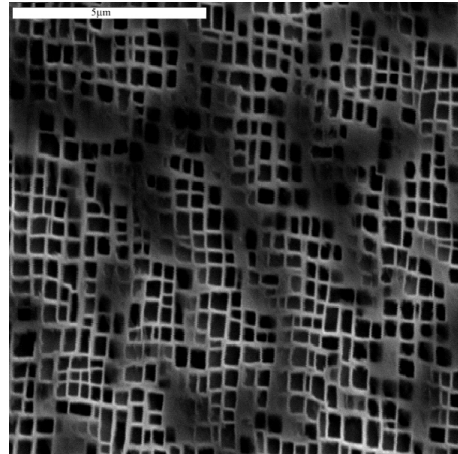


Figure 2c. Microstructure of LDSX-6

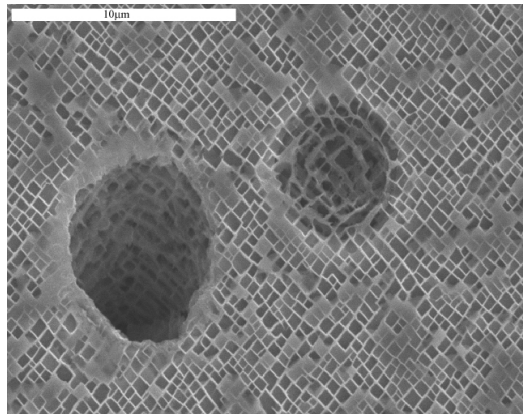


Figure 3. Typical pores in CMSX-4

The average measured widths of the γ' precipitates and γ channels are recorded in Table III.

Table III. Microstructural measurements

| Alloy | Average width of γ' , (μm) | Average width of γ channels (μm) |
|--------|--|--|
| LDSX-5 | 0.36 | 0.136 |
| LDSX-6 | 0.41 | 0.136 |
| CMSX-4 | 0.45 | 0.15 |

All the alloys contained casting pores. A typical example is illustrated in figure 3. These pores played an important role in the observed fatigue behaviour. They will be considered in more detail during the discussion.

Fatigue Procedures

The core fatigue tests were carried out under strain control on a plain cylindrical specimen with a gauge length of 15mm and a nominal 5mm diameter. Two sets of the notched specimens had a DEN (Double Edge Notch) configuration with K_t values of 3.6 and 2.3. The third set had a 'flat plate' geometry with a K_t value of 2.38. The three notch specimens are shown in figure 4.

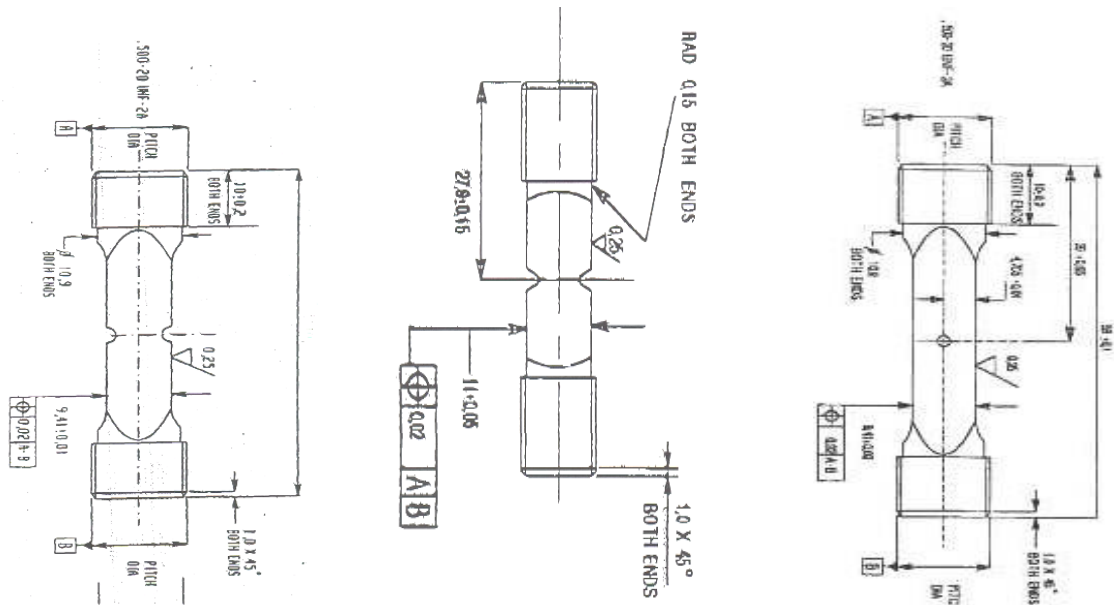


Figure 4. Form and dimensions of the three notch specimens

Additional crack propagation measurements were made on a corner crack specimen with a 7x7mm cross section and a 0.35mm deep slit machined into one corner. The cast bars from which all specimens were machined were aligned so that their primary axis (specimen longitudinal direction) was $<20^\circ$ from [001] direction. An EBSD analysis confirmed that in practice, misalignment amounted to only a few degrees. The analysis also demonstrated that the alignment of notches in the DEN specimens was consistent throughout the whole batch of specimens.

The low cycle fatigue tests complied with the British Standards BS3518: part 1: 1993 for load controlled notch testing and BS7270:1990 for the strain control testing of plain specimens. For all tests a 1-1-1 trapezoidal waveform at a frequency of 0.25Hz was applied. The load control tests were carried out at $R=0$ but the strain control measurements involved both $R=0$ and -1 . The experiments encompassed temperatures of 650°C and 800°C although the majority of the work involved the former. The temperatures were achieved by means of a conventional air furnace with two type K or N thermocouples attached close to the centre of the specimen gauge length. A uniform temperature distribution to within $\pm 1^\circ\text{C}$ was maintained for the duration of the tests. For the strain control experiments, the extensometer, with an extension range of 0.25mm and a position range or gauge length of 10mm, was recalibrated before each test and prior to heating.

The crack propagation tests involved R=-1, 0, -0.5 and 0.5 load ratios and the standard 1-1-1-1 trapezoidal waveform. Crack growth was monitored by a direct current potential difference method in which the constant current was pulsed to minimise heating effects. On conversion of the voltage changes to increases in crack length with cycles, the rate of crack growth (da/dN) was determined by means of a three point secant approach.

All fractured specimens were examined in the SEM to define crack path features including casting pores and their depth below the specimen surface. EBSD was also used to confirm the orientation of all test pieces in relation to notches and crack growth directions.

Experimental Results

Cyclic Stress-Strain Curves

The strain control measurements allowed key material property characteristics to be defined. The important parameters involved monotonic and cyclic yield strengths, ultimate strengths and amount of stress relaxation associated with each temperature. Cyclic stress-strain curves derived from the measured hysteresis loops are illustrated for CMSX-4 and the two alloy variants at 650°C in figure 5a. A similar graph for CMSX-4 at 650°C and 800°C is shown in figure 5b. Given in table IV are the strain hardening rate variables for the 3 alloys at 650°C, based on the data observed in figure 5a.

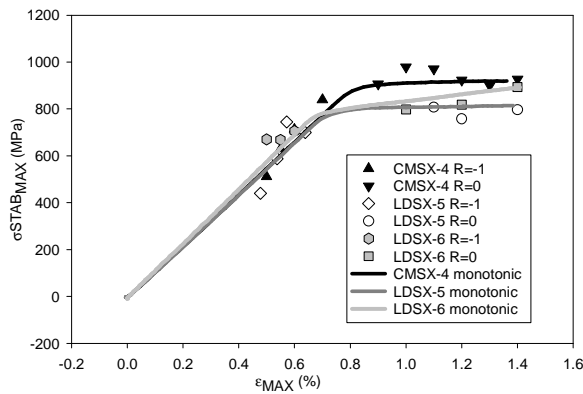


Figure 5a. Monotonic and cyclic stress-strain response of CMSX-4, LDSX-5 and LDSX-6 at 650°C

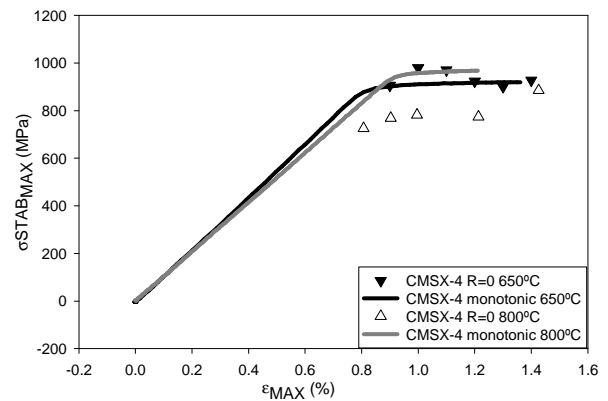


Figure 5b. Monotonic and cyclic stress-strain response of CMSX-4 at 800°C

Table IV. Strain hardening variables.

| Material | K (constant) | n |
|----------|--------------|--------|
| CMSX-4 | 929.1 | 0.0115 |
| LDSX-5 | 815.52 | 0.0105 |
| LDSX-6 | 890.41 | 0.0401 |

Several important deductions can be made from figures 5a and 5b and table IV:

- The monotonic stress-strain curves for CMSX-4 at 650°C and 800°C almost superimpose although there is a slight reduction in modulus with temperature.
- The monotonic strengths of LDSX-5 and 6 are lower than CMSX4 but alloy 6 has a higher rate of strain hardening. This reflects in the LCF notch behaviour (figure 8) as LDSX-6 outperforms the others.
- The CMSX-4 does not cyclically soften at 650°C and in fact tends to cyclically harden.
- In contrast the CMSX-4 at 800°C displays significant cyclic softening
- Both LDSX-5 and 6 at 650°C do not cyclically soften.

Figure 6 illustrates the strain range-life response of CMSX-4 at 650°C and 800°C and the two other variants at 650°C. Upper and lower bound curves have been super-imposed on the graph. The CMSX-4 sits largely in the upper band although there are exceptions. The R=0 data for CMSX-4 at 650 and 800°C generally lie on the dashed line that merges with the upper band. The apparent difference for this alloy between R=-1 and R=0 is not unusual and has been recorded for other systems. LDSX-5 and 6 are generally consistent with the lower band but once again there are exceptions. It is believed that the variability is associated with crack initiation at pre-existing pores. Figure 7 shows the stabilised stress range response of the three alloys at the two temperatures.

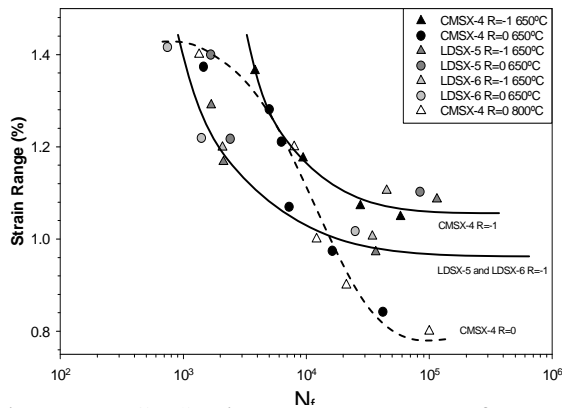


Figure 6. LCF Strain Range response of CMSX-4, LDSX-5 and LDSX-6

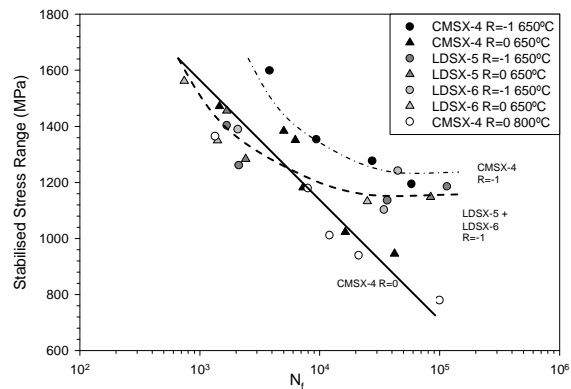


Figure 7. LCF Stabilised Stress Range response of CMSX-4, LDSX-5 and LDSX-6

Notch Fatigue

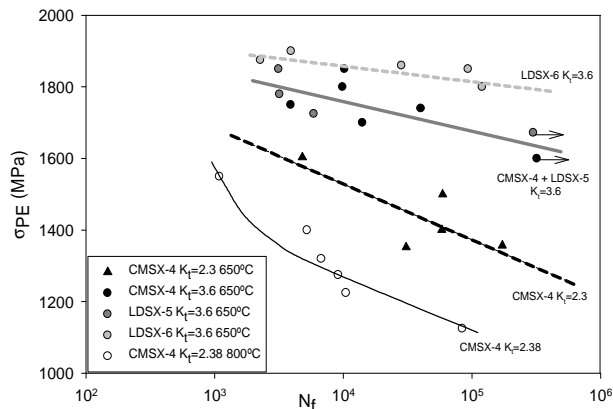


Figure 8. Notch behaviour at 650°C and 800°C for different K_t values

Notch behaviour at 650°C and 800°C is recorded in figure 8. The fatigue data are plotted in terms of peak elastic stress ($K_t \sigma_{nom}$). There is significant scatter particularly at 650°C. This is attributed to the role of casting pores in crack initiation. Even so there are trends. Thus LDSX6 displays a longer life for the $K_t = 3.6$ notches. This may be associated with the higher, monotonic strain hardening characteristic of this alloy. The $K_t=3.6$ data for LDSX5 and CMSX4 effectively superimpose within the observed scatter even though the alloy variant is weaker monotonically and in the strain control experiments. The only common feature of the two alloys is the rate of strain hardening both monotonically and cyclically which would influence the extent of plasticity at the notch root.

Casting Pores and Variability

The test results highlight the role of casting pores in the fatigue performance of both plain and notched specimens. Virtually all fracture surfaces displayed evidence of porosity. However, it was not always evident that a pore was responsible for crack initiation. Some examples of pores and fracture surfaces from strain control specimens are illustrated in figures 9 and 10.

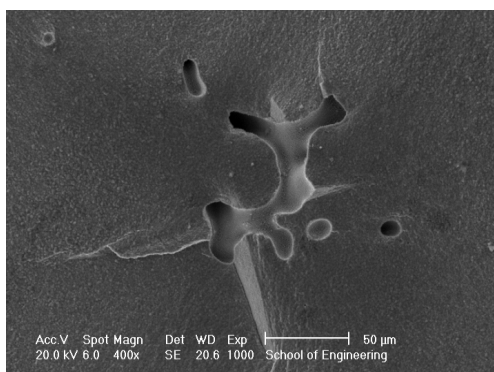


Figure 9. Casting pore in plain CMSX-4 specimen at 650°C

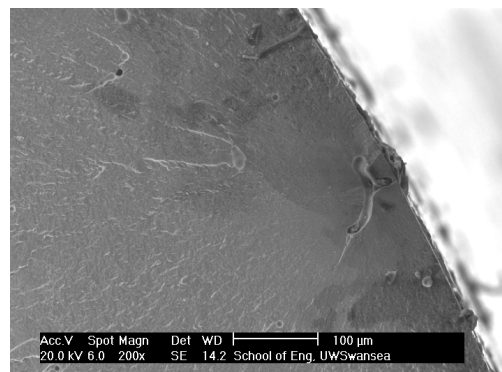


Figure 10. Casting pore in plain LDSX-6 specimen at 650°C

It is believed that the observed variability in fatigue performance is a direct consequence of the pores and their position on the fracture surface. To explore this belief an extensive study was carried out to determine the ligament distance between the pore and the edge of the fracture surface and also the surface area of the pores. Both measurements were achieved by producing a series of images of the respective pores on each test specimen and superimposing ellipse shapes to quantify the size and measurement lines to determine the ligament distance. Figures 11 and 12 illustrate examples of how these measurements were calculated.

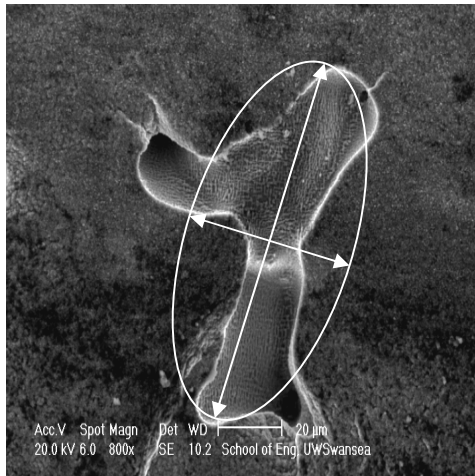


Figure 11. Pore size calculation

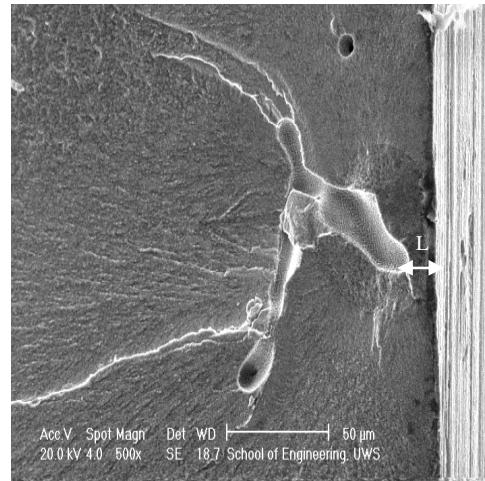


Figure 12. Ligament distance calculation

Figure 11. Area of pore = $\pi \times \frac{1}{2} \text{ length} \times \frac{1}{2} \text{ width} = \pi \times 120\mu\text{m} \times 74\mu\text{m} = 27727\mu\text{m}^2$

Figure 12. Ligament Distance = $13\mu\text{m}$

An additional series of repeat strain control and notch tests were carried out at a strain range of 1% and peak elastic stress of 1750MPa respectively to analyse the effect of porosity. The measured lives together with other supporting information are recorded in Tables V and VI.

Table V. Repeat strain control tests at $\Delta\epsilon=1\%$

| Nf | Peak Stress (MPa) | Stress Range (MPa) | Pore Size (μm^2) | Pore Distance (μm) |
|-------|-------------------|--------------------|-------------------------------|---------------------------------|
| 12311 | 903.9 | 1188.8 | 19905 | 1750 |
| 9983 | 891 | 1172.3 | 7057 | 100 |
| 10997 | 892.8 | 1216.6 | 24328 | 50 |
| 11465 | 1009.1 | 1135 | 5341 | 250 |
| 15894 | 972.4 | 1145.1 | 6231 | 980 |

Table VI. Repeat $K_t=3.6$ notch tests at $K_t\sigma_{max} = 1750$ MPa

| Nf | Ratio | Pore Size (μm^2) | Pore distance (μm) |
|-------|--------|-------------------------------|---------------------------------|
| 4993 | 0.75 | 52 | 39 |
| 50113 | 5.55 | 20 | 111 |
| 8361 | 0.013 | 1227 | 17 |
| 17682 | 0.759 | 362 | 275 |
| 29563 | 0.03 | 1100 | 33 |
| 3899 | 0.0488 | 655 | 32 |

The scatter in lives observed is consistent with the original data in figures 6 and 8. A detailed statistical analysis suggested Weibull distribution functions provide the best fit. For the plain specimens the Weibull ‘ β ’ exponent was unity suggesting an exponential decay in failure rate.

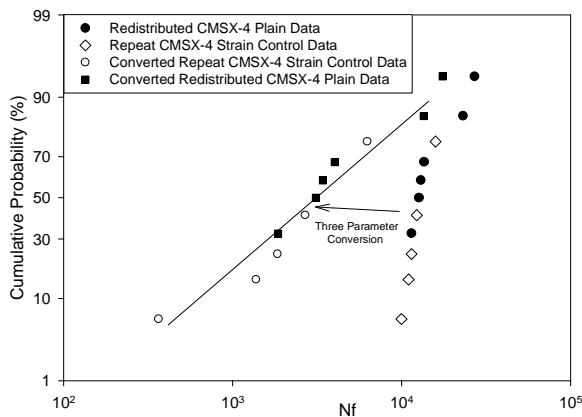


Figure 13. Weibull redistribution in plain CMSX-4 specimens

Tables V and VI also contain measurements made of pore size and pore distance from the specimen outer surface. The pore area was calculated by constructing an elliptical shape around the pore with the major and minor axes matching the extremities of the pore. The areas, therefore, may overestimate pore size but do not take into consideration pore dimensions outside the plane of fracture. It might be anticipated that larger pores and short distance should be associated with shorter fatigue lives. An examination of the two tables demonstrates that reality may not be so straightforward. The histograms in figures 14a and 14b summarise measured areas and pore depths for all the $R=0$ strain control tests at 650°C highlighted in figure 6.

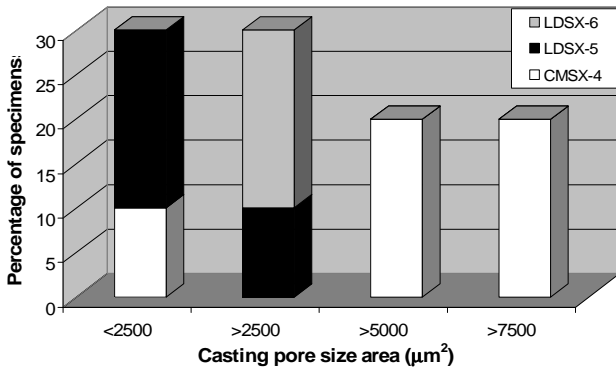


Figure 14a. Critical casting pore area values.

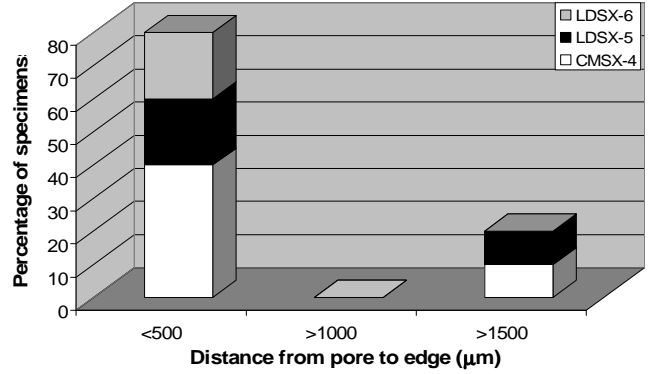


Figure 14b. Critical casting pore ligament distance values.

Discussion

Life Prediction

An objective of the work was to explore the effectiveness of strain approaches in the prediction of notch fatigue response. These methods included the Manson-Coffin [3] relationship and the Walker strain [4] equation with the form

$$\Delta \epsilon_{\text{walker}} = \frac{\sigma_{\text{max}}}{E} \left(\frac{\Delta \epsilon_{\text{actual}} E}{\sigma_{\text{max}}} \right)^m \quad (1)$$

With σ_{max} the maximum cyclic stress at the notch or plain specimen, E the modulus and $\Delta \epsilon_{\text{actual}}$ the strain range experienced. The correlating parameter, m, is obtained by curve fitting plain specimen data at different $R = \left(\frac{\text{min strain or stress}}{\text{max strain or stress}} \right)$ values.

The Walker relationship allows data at different R values to be correlated. Figures 15a and 15b illustrate the Walker predictions of CMSX4 notch data at 650°C ($K_t=2.3$) and 800°C ($K_t=2.38$) based on the strain control results in Figure 6 and the cyclic stress-strain curves in figures 5a and 5b.

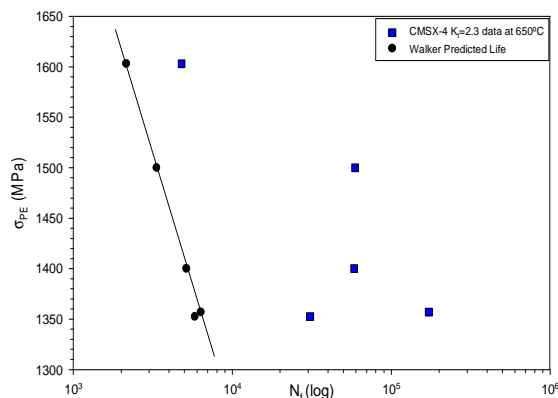


Figure 15a. Walker strain prediction of CMSX4 Kt=2.3 data at 650°C.

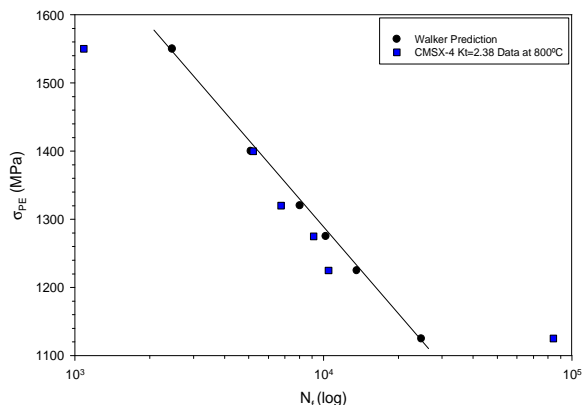


Figure 15b. Walker strain predictions of CMSX4 Kt=2.38 data at 800°C.

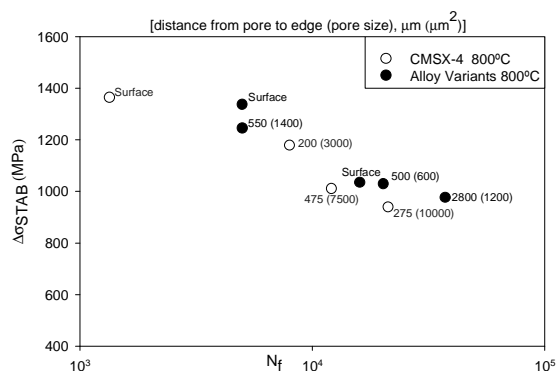


Figure 16. Comparison of surface and subsurface initiation sites in CMSX4 and alloy variants at 800°C.

While the predictions at 800°C are generally acceptable, at 650°C they consistently underestimate measured lives. This discrepancy is attributed to stress conditions associated with the pores. At 800°C, the alloys cyclically soften. This must be due to enhanced dislocation mobility and plastic deformation (figure 5b). It is speculated that as a consequence there will be a significant redistribution of stress thereby diminishing the stress concentration caused by pores. This appears the case in Figure 16 which illustrates plain data at 800°C and summarises initiation sites. Clearly the pores do not degrade the fatigue response with respect to the surface. They, therefore, appear to provide a ‘free’ surface for crack initiation without imposing a significantly higher stress locally.

In contrast, at 650°C the strain control data cyclically hardens. The cyclic response, therefore, tends towards a more elastic response so that any discontinuity in the microstructure acts as a stress raiser. A separate finite element analysis suggests that pores can impose a stress concentration factor ≥ 2 at the pore surface [5]. The under prediction of the notch behaviour through application of the Walker expression is a consequence. The Walker exponent is derived from plain specimen data. Plain specimens have a bigger stressed volume than the notches and hence a greater likelihood of a larger defect. It is, therefore, not surprising that the predicted lives fall short of the measured notch behaviour.

Correlating Pore Impact

It was shown in Tables V and VI that the dependence of fatigue performance on pore size and position is not necessarily straightforward. However, intuitively, fatigue lives should decrease as pore size increases but increase as pore distance (or ligament) from the surface increases. On this basis, the fatigue lives for the repeat plain and notched specimens were expressed in terms of the ratio (ligament/pore area). Thus as the ratio increases the fatigue lives should also increase. The outcome is illustrated in figure 17a for plain specimens and in figure 17b for the notched specimens. The increasing trend is evident. Furthermore correlation coefficients in excess of 0.9 emphasise the strength of the correlation.

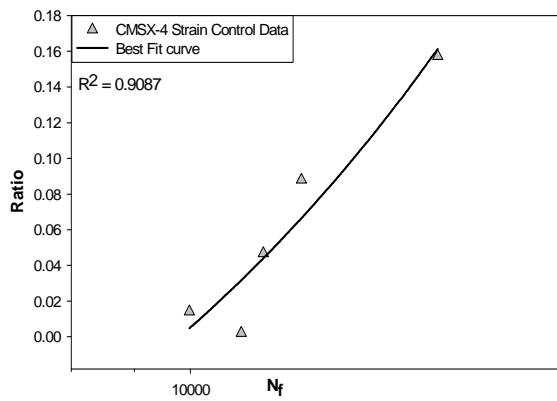


Figure 17a. Ligament / Pore Area Ratio versus life for CMSX-4 plain specimens

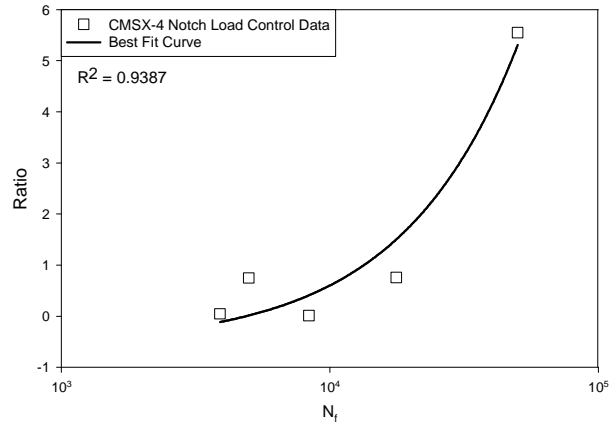


Figure 17b. Ligament/Pore Area Ratio versus life for CMSX-4 $K_t = 3.6$ notched specimens

Damage Tolerance

In general, defect situations are generally assessed by the application of fracture mechanics through equations of the form

$$\frac{da}{dN} = C\Delta K^m \quad (2)$$

With da/dN the rate of crack propagation, C and m constants and ΔK the stress intensity factors [6]. Through integration of this equation, knowledge of m and c from laboratory experiments and an expression for ΔK , the residual lives of specimens and components can be calculated through the following equation.

$$\Delta N = \frac{1}{C\Delta\sigma^m Y^m} \left\{ \frac{a_1^{(1-m/2)} - a_0^{(1-m/2)}}{(1-m/2)} \right\} \quad (3)$$

with Y the geometry term in an expression for the stress intensity factor of the form $\Delta K = Y\Delta\sigma\sqrt{a}$

Brandt [7] has derived a stress intensity expression that is appropriate for the current situation:

$$\Delta K = (0.78 + 0.0395D/L) \Delta \sigma \sqrt{D} \quad (4)$$

which highlights a dependence on ligament distance, L, and pore size, D. For convenience, in the present analysis it was assumed that the initial and developing crack shape was circular with the radius $a = D/2 = \sqrt{\text{pore size}/\pi}$. On this basis, the geometry term has the form

$$Y = \sqrt{2} \{0.78 + 0.0790 a/L\} \quad (5)$$

Since both a and L are changing as the crack grows, the propagation life is calculated incrementally. For each increment the conditions are assumed to be constant. Clearly, a smaller increment size will give a more accurate calculation. On this basis the crack size, a_1 , at the end of an increment of crack growth, ΔN , is given by:

$$a_1 = \left[\Delta N C \Delta \sigma^m Y^m (1 - m/2) + a_0^{(1-m/2)} \right]^{1/m-2} \quad (6)$$

with a_0 the crack size at the start of incremental growth. By summing all the increments, the total crack propagation life can be calculated.

Using this expression and measured crack growth rates at 650°C on CMSX4 corner crack specimens, shown in figure 18, the correlations recorded in table VII was obtained.

Table VII. Calculated crack propagation lives in CMSX4 at 650°C

| Pore Area (μm^2) | Ligament Distance (μm) | m | c | Calculated N_f | Measured N_f |
|-------------------------------|-------------------------------------|------|---------|------------------|----------------|
| 19905 | 1750 | 2.68 | 5.1E-11 | 16063 | 12311 |
| 19905 | 1750 | 2.19 | 4.1E-10 | 4330 | 12311 |

Table VII contains two sets of m and C values. This reflects previously reported work [8] that the rate of propagation is influenced by the direction in which the crack is growing on the (001) plane. This was proven through EBSD analysis as the two R=0 crack propagation tests were shown to have distinctly different orientations. Figures 19a-19d display the (100) and (111) pole figures for the two R=0 tests. Figure 19d shows that the {111} planes in the lower stress test (550MPa) are more favourably orientated for easier shear ahead of the growing crack. Subsequent crack propagation is found to occur on the (100) plane in the <110> direction. In the higher stress specimen, the {111} planes are less favourably aligned and propagation is shown to occur on the (100) plane again but in the <100> direction (see figure 19a), providing a faster rate of propagation. This reflects the comments made by Joyce et al [8], where they found that the <110> direction had a far slower rate of crack propagation due to a higher fatigue crack propagation resistance. Clearly cracks growing from a buried flaw will be influenced by this apparent anisotropy which in turn will impact on the measured lives. The calculated lives span the measured values perhaps reflecting the anisotropic influence.

A further complication in applying crack growth data is the fact that the rate of propagation tends to fluctuate throughout the experimental measurements. This was highlighted by additional tests carried out at 650°C at R ratios of -1, -0.5 and 0.5 at a common maximum

applied stress, figure 20. The oscillation appears to be due to a tendency for the crack to divert onto (111) planes. Figure 21 illustrates the measured growth rate data for the low stress R=0 test while figure 22 shows a section at 45° through the crack for the same specimen. Figure 23 demonstrates the associated crack branching on the fracture surface of a notched specimen and finally figure 24 shows that essentially the shear conditions on the (111) plane can become critical thereby promoting ultimate fracture.

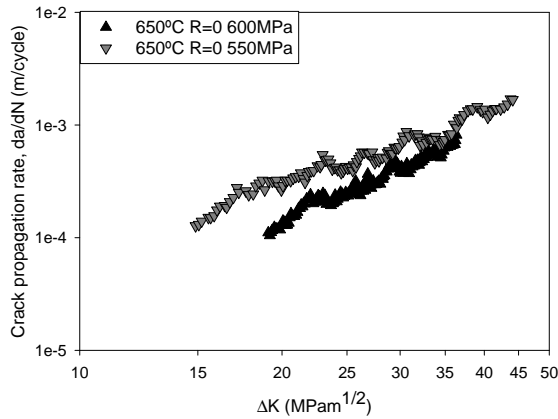


Figure 18. Crack Propagation rates for CMSX-4 at 650°C at R=0.

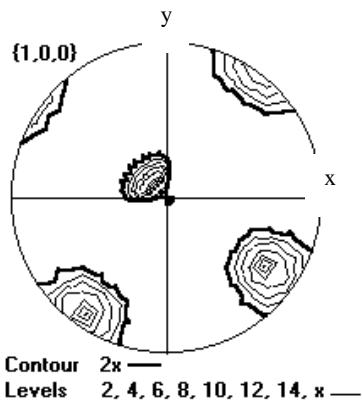


Figure 19a. (100) pole figure for high stress test

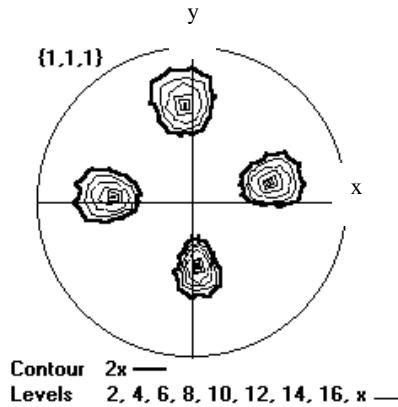


Figure 19b. (111) pole figure for high stress test

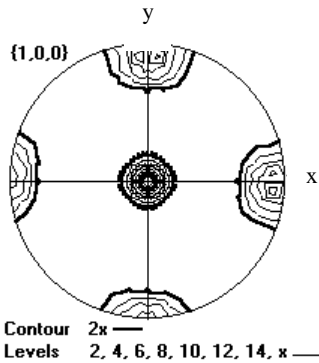


Figure 19c. (100) pole figure for low stress test

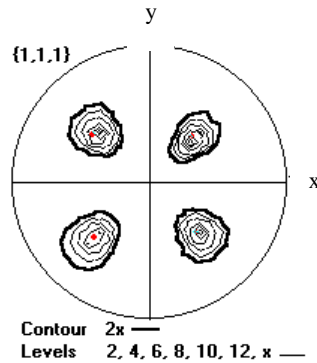


Figure 19d. (111) pole figure for low stress test

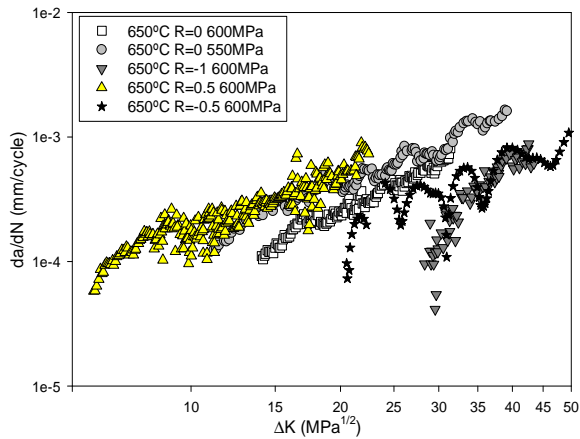


Figure 20. Crack Propagation rates for CMSX-4 at 650°C.

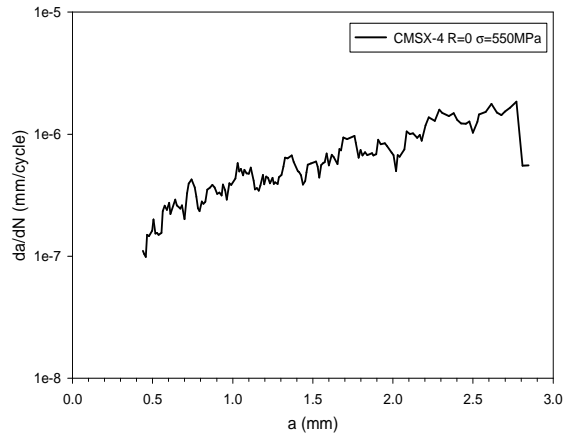


Figure 21. Crack propagation behaviour in CMSX-4 R=0 low stress test (550MPa).

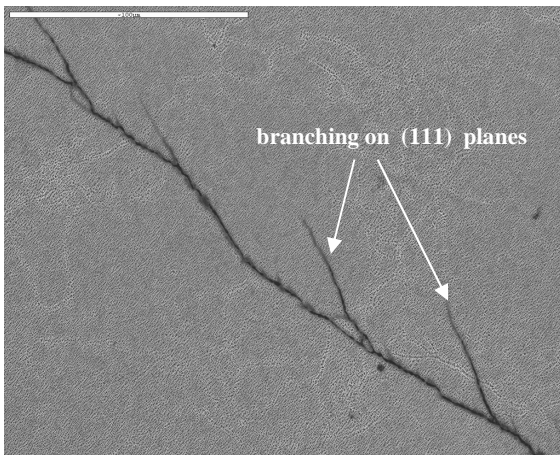


Figure 22. Crack Growth in CMSX-4 R=0 specimen (low stress = 550MPa).

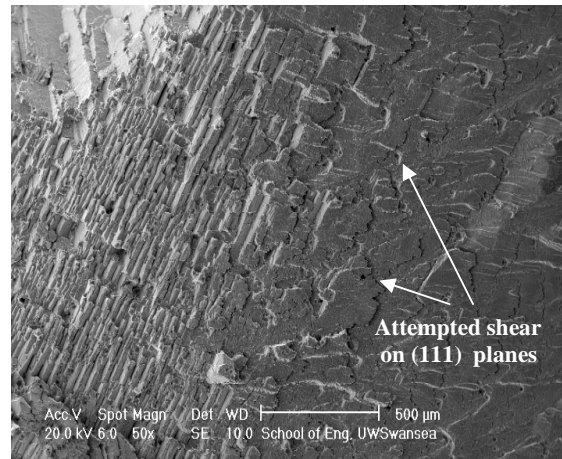


Figure 23. Evidence of attempted shear on (111) planes in a notched specimen.

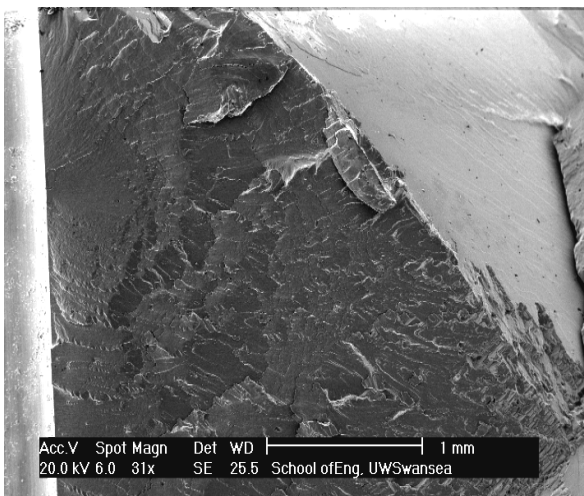


Figure 24. Final shear on a (111) plane in a Notched specimen

Conclusions

The paper explores the strain control fatigue behaviour of CMSX4 and several alloy single crystal variants. It clearly demonstrates differences in the cyclic fatigue response at 650°C and 800°C which are related to increased dislocation mobility at 800°C. The different response impacts on the role that casting pores play in the initiation of fatigue cracks. This is illustrated through application of the Walker strain relationship which is effective at 800°C but under predicts notch lives at 650°C possibly because of ‘weak’ link concepts associated with volume differences. Two approaches to the life prediction of the pores are discussed. One correlates the fatigue lives to the ratio ligament distance to pore area. The second demonstrates the effectiveness of fracture mechanics and the application of crack growth data in calculating residual propagation lives. Potential problem areas with the latter include an orientation dependence of crack growth rates and a tendency for oscillation in crack growth rates due to branching on (111) planes.

Acknowledgements

The authors gratefully acknowledge the support and assistance given by Rolls-Royce plc in this work and for the DARP funding from the EPSRC.

References

1. P.J. Hurley, M.T. Whittaker, S.J. Williams and W.J. Evans, “Prediction of fatigue initiation lives in notched Ti 6246 specimens,” *International Journal of Fatigue*, 30(2008), 623-634.
2. W.J. Evans, J.P. Jones and S.J. Williams, “The interaction between fatigue, creep and environmental damage in Ti6246 and Udimet 720Li”, *International Journal of Fatigue*”, 27(2005), 1473-1484.
3. S.S. Manson, “Fatigue: a complex subject – some simple approximations,” *Exp. Mech.*, 5(1965), 193-226.
4. K. Walker, “Effects of environment and complex load history on fatigue life,” *ASTM STP* 462(1970) 1-14.
5. W.J. Evans, N. Mohd Shariff and P.J. Nicholas, “Fatigue behaviour of cast and powder metallurgy aluminium-based metal matrix composites,” *Fatigue 2002*, 3(2002), 1897-1904. Proceedings of the Eighth International Fatigue Congress.
6. P.C. Paris and F. Erdogan, A critical analysis of crack-propagation laws, *Journal of Basic Engineering*”, 85(1963), 528-534.
7. D.E. Brandt, “The development of a turbine wheel design criterion based on fracture mechanics,” *Journal of Engineering for Power, Trans. ASME*, 93(1971), 411.

8. M.R. Joyce, X Wu, P.A.S. Reed, "The effect of environment and orientation on fatigue crack growth behaviour of CMSX-4 nickel base single crystal at 650°C," *Materials Letters*, 58(2003), 99-103.

The authors gratefully acknowledge the support and assistance given by Rolls-Royce plc in this work and for the DARP funding from the EPSRC.